

How many Raman-active vibrations do exist in carbon nanotubes?

T. Yu. Astakhova, and G. A. Vinogradov

Institute of Biochemical Physics RAS, ul.Kosygina 4, Moscow GSP-1 119991, Russia

E-mail: astakhova@deom.chph.ras.ru; gvin@deom.chph.ras.ru

Abstract

In this paper we present the results on Raman-active modes calculation in achiral (n, n) and $(n, 0)$ carbon nanotubes (CNTs). vibrational spectra are derived as the eigenvalues of corresponding dynamical matrix at the Γ -point of Brillouin zone. Diagonal components and α_{xy} ($= \alpha_{yx}$) are the only non-zero components of polarization tensor. Selection rules for Raman-active modes are determined by direct estimations of matrix elements responsible for the intensities of corresponding vibrational transitions. Few E_{2g} modes can be non-Raman-active because of their “fine” vibrational structure. We claim that numbers of Raman-active modes for achiral CNTs are: 5 ((n, n) and $(n, 0)$, n -even); 6 ((n, n) , n -odd); 8 ($(n, 0)$, n -odd).

I. INTRODUCTION

Carbon nanotubes (CNTs) are highly organized quasi-one-dimensional structures consisting of rolled-up graphene sheets. The variations in their diameters and helicities result in differences in electronic and vibrational properties [1], [2], with Raman spectroscopy providing a powerful tool for their characterization. Currently, a few problems still exist in the calculation of the full list of Raman-active vibrations and their symmetry assignments. For some time it was believed that there were 15 or 16 Raman vibrations for achiral $(n, 0)$ and (n, n) CNTs depending on whether n is odd or even [3]. The group-theoretical analysis

predicts 7 intensive Raman-active vibrations in the range up to 1600 cm^{-1} [4]. Decomposition of experimentally observed spectra into individual components was made following this predictions [5], [6].

Recently the total number of Raman-active vibrations was declared to be half of the previous estimates, namely 8 for both armchair and zigzag CNTs [7]. The corresponding calculations are based on the rod (or line) group theory [8], worked out earlier for the stereoregular polymers [9].

In the present work we perform a detailed analysis of the vibrational spectra of infinite CNTs with a view to address the unresolved issues. Our approach differs from the conventional approach, where the point and spatial symmetry groups are assigned first, followed by the full spectral analysis. Calculations are performed using Brenner's empirical potential for hydrocarbons [10]. Infinite CNTs are simulated by supercells with periodic boundary conditions. The full set of normal vibrational modes is obtained by the diagonalization of the dynamical matrix. The mode symmetries are assigned according to commonly accepted rules [11], [12], [13]. Selection rules for Raman-active modes are found by an estimation of matrix elements responsible for the intensity of the corresponding mode. The estimation is based on the direct comparison of the mode symmetry with the symmetry of polarization tensor components in polar coordinates. This approach does not require the preliminary complete group-theoretical analysis of CNTs. Nevertheless, the necessary symmetry assignment of vibrational modes is made.

In this paper we present results for armchair (n, n) and zigzag $(n, 0)$ CNTs with $n = 9 - 12$. The detailed analysis of the vibrational modes demonstrates that there can be modes with identical symmetries that give different contributions to Raman spectra. It follows from the difference in the "fine" structure of these modes, and depends on whether vibrations of neighboring atoms are "in-phase" or "out-of-phase".

The manuscript is organized as follows: In the second section we present the details of the construction and analysis of the dynamical matrix. Sec. III sketches the symmetry properties of achiral nanotubes. Sec. IV provides a brief description of the general rules for the estimation of the Raman-active vibrations. In Sec. V we present results for achiral

tubes (n, n) and $(n, 0)$ where the vibrational spectrum of a $(10, 10)$ nanotube is analyzed in more details as an example. Sec. VI provides a summary of our results.

II. CALCULATION OF VIBRATIONAL SPECTRUM USING THE DYNAMICAL MATRIX.

The vibrational spectrum can be derived as the solution of the matrix equation:

$$\mathbf{D} X = M \omega^2 \mathbf{B} X, \quad (1)$$

where \mathbf{D} is the dynamical matrix and \mathbf{B} is the matrix of coefficients of quadratic form of kinetic energy $E_{kin} = \frac{1}{2} \sum b_{ij} v_i v_j$, (v_i, v_j are generalized velocities of atoms i and j). $\{\omega_k\}$ and $\{X_k\}$ are, respectively, the eigenvalues and eigenvectors fully describing the vibrational spectrum. M is the mass of carbon atom. Matrix elements \mathbf{D}_{ij} are given by:

$$\mathbf{D}_{ij}^{\alpha\beta} = \frac{\partial^2 E}{\partial \alpha_i \partial \beta_j}, \quad (2)$$

where E is the potential energy of the system; α_i, β_j are generalized coordinates of atoms i and j . In Cartesian coordinates \mathbf{B} in (1) is the unit matrix and vibrational spectrum is obtained by diagonalization of matrix \mathbf{D} . Corresponding eigenvectors contain all information on symmetry and relative amplitudes of atomic displacements from the equilibrium. The Brenner's potential [10] is used for modeling nanotube structure and vibrational properties. Analytical form of this potential allows to get second derivatives analytically. Cylindrical coordinates greatly facilitate the construction of the dynamical matrix: it is sufficient to calculate the matrix elements for two neighboring atoms and then the dynamical matrix is reconstructed by symmetry. The aspect ratio of CNTs is very large and it allows to consider the CNTs as infinite. We use a supercell with periodic boundary conditions to model the infinite tube.

If a supercell consists of N atoms, the rank of the dynamical matrix is $3N \times 3N$ and Eqn. (1) has $3N$ solutions giving the full set of normal vibrations. We consider modes only in the center of the Brillouin zone (Γ -point with $k_z = 0$). Modes with $k_z \neq 0$ give contribution to Raman-spectra for finite CNTs [14], [15], and will be omitted in the present

consideration. As a result, the rank of the dynamical matrix decreases to $3 N' \times 3 N'$, where $3 N'$ is the number of vibrations with $k_z = 0$.

The symmetry assignments are standard (see, *e.g.*, [11], [12], [13]). For one-dimensional representations letters A and B stand for symmetric and antisymmetric modes with respect to S_{2n}^1 symmetry operations; subscripts ‘1’ and ‘2’ - denote symmetric and antisymmetric modes with respect to the rotation about two-fold axes perpendicular to the principal axis. The letters ‘ g ’ and ‘ u ’, - symmetric and antisymmetric modes with respect to the inversion. In two-dimensional representations E_k , the subscript k stands for modes which transform to itself by the S_{2n}^k symmetry operation. An advantage for the choice of S_{2n} as the principal axis over the C_n axis for CNTs is given in Sec. V. The results are summarized in Tables I, II and will be discussed below.

There are A and B modes with “double” symmetries with respect to the rotation about C_2 axes perpendicular to the principal axis S_{2n} . An example of such (Raman-inactive) mode in (n, n) CNT with even n is given in Fig. 1. The mode shown is the B_g tangential mode where all atoms in every layer¹ have equal displacements. There are three classes of C_2 rotational axes perpendicular to the tube axis (C_2' , C_2'' , C_2''') for even n . (More detailed analysis of CNT symmetry elements will be given in the next Section). One can see that mode B_g is antisymmetric with respect to C_2' and C_2'' axes and is symmetric with respect to C_2''' axis. This is the reason why subscripts ‘1’ or ‘2’ are omitted for some A and B modes in Table I.

Following these rules, the symmetry analysis shows that the vibrational modes of (n, n) and $(n, 0)$ CNTs with even and odd n have following symmetries:

¹All atoms with equal z-coordinates form a layer.

$$\begin{aligned}
\Gamma_{(n,n)}^{n\text{-even}} &= 2 A_{1g} + 2 A_{2g} + 2 A_u + 1 B_{1u} + 1 B_{2u} + 4 B_g + \\
&\quad 2 E_{1g} + 4 E_{1u} + 4 E_{2g} + 2 E_{2u} + \dots + 2 E_{(n-1)g} + 4 E_{(n-1)u} \\
\Gamma_{(n,n)}^{n\text{-odd}} &= 2 A_{1g} + 2 A_{2g} + 2 A_g + 1 B_{1u} + 1 B_{2u} + 4 B_u + 6 E_{1u} + 6 E_{2g} + \dots + 6 E_{(n-1)g} \\
\Gamma_{(n,0)}^{n\text{-even}} &= 2 A_{1g} + 1 A_{2g} + 3 A_u + 1 B_{1u} + 2 B_{2u} + 3 B_g + \\
&\quad 3 E_{1g} + 3 E_{1u} + 3 E_{2g} + 3 E_{2u} + \dots + 3 E_{(n-1)g} + 3 E_{(n-1)u} \\
\Gamma_{(n,0)}^{n\text{-odd}} &= 2 A_{1g} + 1 A_{2g} + 3 A_g + 1 B_{1u} + 2 B_{2u} + 3 B_u + 6 E_{1u} + 6 E_{2g} + \dots + 6 E_{(n-1)g}
\end{aligned} \tag{3}$$

Four zero-frequency modes are not shown in (3). The rotation about z -axis has A_{2g} symmetry (see Fig. 2a); the translation along the z -axis has B_{2u} symmetry ²; translations in (x, y) plane are doubly-degenerated and have E_{1u} symmetry (Fig. 2c). Symmetries of zero-frequency modes differ from symmetries given in [2] because we use S_{2n} as the principal axis.

Before proceeding with the analysis of the Raman-activity of calculated vibrational modes we briefly recall the main symmetry elements in CNTs.

III. SYMMETRY ELEMENTS IN CNTS.

An analysis of the vibrational modes and comparison with polarization tensor components requires a knowledge of necessary symmetry elements of CNTs. Note that the symmetry analysis is independent on the form of interatomic potential; this choice determines only frequencies but not symmetries.

The full group-theoretical analysis of CNTs is beyond the scope of this work ³. A list of

² B symmetry is assigned because this mode is antisymmetric with respect to S_{2n}^1 operation which is a rotation by an angle $2\pi/2n$ and reflection in the horizontal plane passing through centers of the slanted bonds. If the C_n axis is taken as the principal axis then this mode has A_{2u} symmetry since it is symmetric with respect to the C_n^1 rotation (Fig. 2b)

³One can find the group-theoretical analysis in [7], and nonsymmorphic rod-group is:

allowed point symmetry elements for (n, n) CNTs with even and odd n is given in Table III. Symmetry elements for D_{nh} and D_{nd} point groups are also shown for comparison.

Fig. 3 illustrates symmetry operations for (n, n) CNTs with even and odd n ($n = 6$ in Fig. 3a, and $n = 5$ in Fig. 3b). Two different forms of unit cells are used, since different symmetry elements are clarified in different representations. Two top panels show chains of hexagons chosen as unit cells. Top panel in column (b) (odd n) shows a two-fold rotation axes, C'_2 , passing through centers of a hexagon and an opposite horizontal bond. This axis splits into two classes of two-fold rotation axes for even n , as shown in the top panel of column (a). One rotation axis, C'_2 , passes through centers of opposite hexagons, while the other, C''_2 , passes through centers of opposite horizontal bonds. The (n, n) CNT with even n is thus associated with two classes of reflection planes: σ'_v and σ''_v passing through C'_2 and C''_2 axes, respectively. By contrast, there is only one class of reflection planes, σ'_v associated with a CNT with odd n . Moreover, while the point i in the top panel for even n is an inversion center, the corresponding point O' in the right panel is not an inversion center. Two top panels also show that both tubes have horizontal reflection planes σ_h passing through centers of hexagons.

In order to illustrate other symmetry elements we show the armchair fragments as the unit cell for both tubes in middle panels in Fig. 3. One can see that there are additional two-fold rotation axes, C'''_2 , passing through centers of opposite slanted bonds. Additionally, both tubes have $2n$ -fold roto-reflection axes, S_{2n} . The inversion center in the case of odd n (right panel) is i and inversion is absent for even n .

The bottom panels in Fig. 3 are the side view of both tubes with corresponding symmetry elements.

To summarize: there are symmetry elements, C_n , S_{2n} , σ_v , C'''_2 , as well as two types of fixed points, i (inversion) and O , which are common to CNTs with both even and odd n . Symmetry elements C'_2 , C''_2 , σ'_v , σ''_v are inherent to CNTs with even n , while elements C'_2

$$G[n] = L_{T_z} \times \left[D_{nh}|_{z=0} \otimes \left(D_{nd}|_{z=T_z/4} \oplus C_{nv} \right) \oplus C_{nv} \times S_{2n} \right].$$

and σ'_v are characteristic to odd n .

This analysis also demonstrates that all symmetry elements of both D_{nd} and D_{nh} groups are permitted in CNTs (see Table III and Fig. 3). One can say that CNTs ‘combine’ symmetry properties of D_{nh} and D_{nd} point groups. In particular, CNT has three classes of two-fold axes for even n : (C'_2, C''_2, C'''_2). These axes are the combination of two classes for D_{nh} symmetry group (C'_2, C''_2 axes) and one class of C_2 axes for D_{nd} (C'''_2 axes).

In the case of zigzag CNTs an analysis is similar. Thus, with a knowledge of CNTs symmetry elements and the calculated vibrational spectra we can identify Raman-active modes in CNTs.

IV. HOW TO REVEAL RAMAN-ACTIVE MODES?

In this Section we recall main rules for determining Raman-active modes. Let the transition between states E_i and E_j is associated with wave functions ψ_i and ψ_j . Then the probability for the $\psi_i \rightarrow \psi_j$ process is proportional to the square of the transition moment M_{ij} , where

$$M_{ij} = \int \psi_j^* M \psi_i dV. \quad (4)$$

In Raman process, M is the dipole moment induced by the external field \vec{E} . The induced dipole moment is $\vec{P} = \alpha \vec{E}$, where α is a polarization tensor. Thus, the selection rules in Raman spectra are determined by the values of integrals

$$\int \psi_j^* \alpha_{\xi\xi'} \psi_i dV, \quad (5)$$

where $\alpha_{\xi\xi'}$ is a component (or a linear combination of components) of the polarization tensor ($\xi, \xi' = x, y, z$). The transition $i \rightarrow j$ is allowed if (5) is nonzero for at least one component $\alpha_{\xi\xi'}$. The integration is performed over the full set of electronic and nuclear coordinates. Direct calculation of (5) is very complicated problem. So, the usual practice is to consider the electronic, vibrational and rotational degrees of freedom separately. Thus the wave function can be written as the product $\psi = \psi^{el} \psi^{vib} \psi^{rot}$. As a result only the following integrals should be estimated for Raman transitions:

$$\int \psi_j^{vib} \alpha_{\xi\xi'} \psi_i^{vib} dV. \quad (6)$$

vibrational wave function ψ^{vib} is real and is represented by an eigenvector of the dynamical matrix. Since we consider the Γ -point of Brillouin zone, where the dependence on the z coordinate is absent, the space integration in (6) is replaced by the area integral

$$\int \psi_j^{vib} \alpha_{\xi\xi'} \psi_i^{vib} dx dy. \quad (7)$$

It is convenient to return back to the polar coordinates $(\xi, \xi' = r, \phi)$. In the simplest case the ground-state vibrational mode ψ_i is fully symmetric and is a constant in polar coordinates. Moreover, the vibrational wave function is the discrete function (eigenvector of the dynamical matrix). Then (7) transforms to the sum:

$$\sum_{m=1}^{2n} \psi_j^m \alpha_{\xi\xi'}, \quad (8)$$

where the summation is over atoms m , $m = 1, 2, \dots, 2n$ of only one layer, and products of polarization tensor components with m -th elements ψ_j^m of eigenvector of j -th normal mode are calculated for angles ϕ^m , corresponding to polar coordinate of atom m . This approach is very convenient as both polarization tensor components and eigenvector elements of vibrational modes have very simple representation in polar coordinates for CNTs.

As is demonstrated in Appendix, only α_{xx} , α_{yy} , $\alpha_{xx} \pm \alpha_{yy}$ and α_{xy} components of polarization tensor differ from zero for CNTs and are shown in Fig. 4.

Many one-dimensional modes in (3) can be excluded from candidates for Raman vibrations. (i) All modes with subscript ‘u’ are eliminated as all components of polarization tensor are symmetric with respect to this operation; (ii) All B modes are excluded as antisymmetric with respect to S_{2n} operation. (iii) A_{2g} modes are also non-Raman-active as they are asymmetric with respect to C_2 operations. Hence, only two fully symmetrical A_{1g} modes are Raman-active.

Doubly-degenerated E_{kg} modes in polar coordinates behave as $\sin(k\phi + \psi)$, where ψ – some phase. Their schematic view is given in Fig. 5. The signs assignment is arbitrary. For instance, the clockwise direction for tangential displacements and radial displacements out of center have ‘+’ sign.

Comparison of Fig. 4 and Fig. 5 results in the fact that only E_{2g} mode can be Raman-active. Really, the shapes of components of polarization tensor coincide only with the shape of E_{2g} mode, and signs of their lobes alternate in the same manner. Actually, it is necessary to estimate expression (7), which can be reduced to

$$\int_0^{2\pi} \sin(2\phi + \theta) \sin(k\phi + \psi) d\phi, \quad (9)$$

and is different from zero only if $k = 2$. ($\sin(2\phi + \theta)$ is the general representation for α_{xy} and $\alpha_{xx} - \alpha_{yy}$ components of polarization tensor, and phases ψ – for vibrational modes and θ – for polarization tensor are related as their principal axes coincide.) It means that only E_{2g} modes can be Raman-active. The conclusion that only A_{1g} and E_{2g} modes are Raman-active is valid for all types of achiral CNTs, both armchair and zigzag with arbitrary n (see Table II).

V. RAMAN-ACTIVE MODES IN ACHIRAL CNTS

Two A_{1g} modes for all types of CNTs are Raman-active as they are fully symmetrical “breathing” and tangential modes (see Fig. 6). Now we will demonstrate that one of E_{2g} modes is not Raman-active on the example of (10, 10) CNT. All E_{2g} modes are shown in Fig. 7. One can see the difference between mode (c) and three other modes, this difference being in ‘signs’ of relative displacements of neighboring atoms. These displacements are predominantly “in-phase” for (a), (b) and (d) modes and are “out-of-phase” for (c) mode. Hence, these “phase” relations of different modes give different contributions to (8): this sum is not equal to zero for modes (a), (b), (c) and is zero (or very close to zero) for mode (d). It means that mode (c) is not Raman-active, and Raman spectra of (10, 10) CNT have 5 Raman-active vibrations (see Table II). This conclusion is valid for all (n, n) CNTs with even n .

Situation with E_{2g} vibrations for (n, n) CNTs with odd n is analogous. Among six E_{2g} modes there are two “out-of-phase” modes which are not Raman-active, and total number of Raman-active vibrations in this type of CNTs is 6.

There are no “out-of-phase” modes in $(n, 0)$ CNTs, and the total number of Raman-active vibrations is the sum of A_{1g} and E_{2g} mode types: 5 Raman-active modes for $(n, 0)$ CNTs if n is odd, and 8 Raman-active modes if n is even.

The reason why armchair CNTs differ from zigzag CNTs consists in the fact that the latter have one atom in the primitive cell, and the former – two atoms. Two atoms in the primitive cell for armchair CNTs allow intrinsic vibrational “fine” structure. Qualitatively it can be demonstrated as follows.

We consider E_{kg} modes, and the armchair ring is chosen as the unit cell. This unit cell consists of $4n$ atoms from two layers (see Fig. 8a, where $(6, 6)$ CNT is shown, as an example). Let us open this fragment into a planar structure (Fig. 8b) and further project into a linear chain (Fig. 8c). There are two atoms in the primitive cell (two adjacent atoms in a layer) since S_{2n} axis was chosen as a principal axis. So every filled circle in Fig. 8c represents one primitive cell of two atoms. This gives a chain with cyclic boundary conditions consisting of $n_c = 2n$ units, and its solution is convenient to write in the form:

$$u(k, l) = a \cos(2\pi k l / n_c), \quad (10)$$

where $u(k, l)$ is a deviation of the unit l for k -th type of normal vibration ($k = 0, 1, \dots, n_c - 1$), and l numerates the units in the chain ($l = 1, 2, \dots, n_c$).

So, the full vibrational spectrum of (n, n) CNT in the center of the Brillouin zone can be approximated by a solution of the one-dimensional chain with cyclic boundary conditions and some effective potential.

The solution (10) gives all one- and two-dimensional modes. Really, if $k = 0$ then all units have equal deviations $u(0, l) = a$ of the same sign, which corresponds to A modes. If $k = n_c/2$ then all units have equal absolute values of deviations, but the signs of relative deviations alternate $u(n_c/2, l) = (-1)^l a$, which corresponds to B modes.

Modes E_{kg} are formed by pairs of solutions (10) with ‘conjugated’ values of k : k and $n_c - k$. Really,

$$a \cos(2\pi (n_c - k) l / n_c) = a \cos(2\pi k l / n_c),$$

and it gives $(n - 1)$ E_{kg} modes for (n, n) CNTs in agreement with (3).

The solution (10) for $k = 2$ is shown in Fig. 8c and corresponds to E_{2g} mode of the nanotube. This mode can be represented schematically in polar coordinates as shown in Fig. 8d and is equivalent to mode E_{2g} in Fig. 5.

VI. CONCLUSIONS

The main goal of the present communication is the calculation of numbers of Raman-active modes in achiral CNTs (n, n) and $(n, 0)$ ($n = 9-12$). vibrational modes are calculated in Γ -point of Brillouin zone, and Raman-active modes are identified by an estimation of matrix elements responsible for the intensity of corresponding transitions, and no preliminary full group-theoretical analysis of CNTs is necessary in this case. For achiral CNTs only three diagonal and $\alpha_{xy} = \alpha_{yx}$ components of polarization tensor are not equal to zero.

We have shown that there are one or two E_{2g} modes for (n, n) CNTs which are not Raman-active. It follows from the fact that the primitive cell of these CNTs has two atoms, and vibrational modes have “in-phase” and “out-of-phase” types of vibrations, the latter being non-Raman-active. The primitive cell of $(n, 0)$ CNTs consists of one atom and these CNTs has no analogous complications.

The calculated numbers of Raman-active modes are five or six for (n, n) CNTs for even and odd n , correspondingly. For $(n, 0)$ CNTs there are five Raman-active modes for even n and eight Raman-active modes for odd n .

Our primary goal was to formulate the selection rules for Raman-active modes and less attention was paid to calculations of mode frequencies. More precise values of mode energies can be obtained using more sophisticated potentials, it e.g. Menon’s tight-binding scheme [16], [17].

The authors thank the RFBR (Project 02-02-16205) and INTAS (Project 00-237) for the partial financial support. T.A. is also indebted to RFBR (Project 00-15-97334). Stimulating discussions with M.Menon, E.Richter, L.A.Gribov, and B.N.Mavrin are gratefully acknowledged.

APPENDIX A: POLARIZATION TENSOR COMPONENTS FOR CNTS

1) We consider non-resonance Raman transitions. For simplicity achiral CNT are represented as homogeneous hollow cylinder of sufficiently large radius.

2) Let external electric field is applied along the x -axis perpendicular to the vertical nanotube axis z . This field can not induce polarization along z -axis as the “top” and the “bottom” of CNT are equivalent. By symmetry the same is valid for y -direction of applied field. Hence, $\alpha_{xz} = \alpha_{zx} = \alpha_{yz} = \alpha_{zy} = 0$.

3) Now we define the angular dependence of components α_{xx} and α_{xy} in polar coordinates. External electric field is aligned along the x -axis and we consider the (xy) section of CNT (see Fig. 9). Polarization vector at point A , ($\phi = 0$) has only normal component: $\vec{P}_n = \alpha_n \vec{E}$, and α_n is the normal polarizability. There is only tangential component at point B ($\phi = \pi/2$) and $\vec{P}_\tau = \alpha_\tau \vec{E}$, where α_τ – tangential polarizability. Obviously, $\alpha_\tau > \alpha_n$ as polarizability in the plain is larger compared to perpendicular direction.

4) Consider now point C at an angle ϕ to x -axis. Electric field at this point has normal ($E_n = E \cos \phi$) and tangential ($E_\tau = E \sin \phi$) components. Normal and tangential components of polarization vector at this point are:

$$\begin{cases} P'_n = \alpha_n E \cos \phi \\ P'_\tau = \alpha_\tau E \sin \phi \end{cases}, \quad (\text{A1})$$

and x - and y -components of polarization vector \vec{P}' at point C are:

$$\begin{cases} P'_x = P'_n \cos \phi + P'_\tau \sin \phi \\ P'_y = P'_n \sin \phi - P'_\tau \cos \phi \end{cases} \quad (\text{A2})$$

Substituting in system (A2) values for P'_n and P'_τ from (A1) one gets:

$$\begin{cases} P'_x = (\alpha_n \cos^2 \phi + \alpha_\tau \sin^2 \phi) E \\ P'_y = (\alpha_n \sin \phi \cos \phi - \alpha_\tau \sin \phi \cos \phi) E \end{cases} \quad (\text{A3})$$

And it follows that

$$\begin{cases} \alpha_{xx} = \alpha_n \cos^2 \phi + \alpha_\tau \sin^2 \phi \\ \alpha_{xy} = -\frac{1}{2} (\alpha_\tau - \alpha_n) \sin 2 \phi \end{cases} \quad (\text{A4})$$

One can get expressions for other non-zero components of polarization tensor in polar coordinates:

$$\left\{ \begin{array}{l} \alpha_{yy} = \alpha_{\tau} \cos^2 \phi + \alpha_n \sin^2 \phi \\ \alpha_{xx} + \alpha_{yy} = \alpha_{\tau} + \alpha_n \\ \alpha_{xx} - \alpha_{yy} = (\alpha_n - \alpha_{\tau}) \cos 2\phi \end{array} \right. \quad (\text{A5})$$

Schematic view of all non-zero components of polarization tensor is shown in Fig. 4.

REFERENCES

- [1] M.S.Dresselhaus, G.Dresselhaus, and P.C.Eklund, *Science of Fullerenes and Carbon Nanotubes* (Academic Press, San Diego, 1996).
- [2] R.Saito, G.Dresselhaus, and M.S.Dresselhaus, *Physical Properties of Carbon Nanotubes* (Imperial College Press, London, 1998).
- [3] R.A.Jishi, L.Venkataraman, M.S.Dresselhaus, and G.Dresselhaus, *Chem.Phys.Lett.*, **209**, 77 (1993).
- [4] R.Saito, T.Takeya, T.Kimura, G.Dresselhaus, and M.S.Dresselhaus, *Phys.Rev.B*, **57**, 4145 (1998).
- [5] A.M.Rao et al., *Science*, **275**, 187 (1997)
- [6] C.Journet et al., *Nature (London)*, **388**, 756 (1997).
- [7] O.E.Alon, *Phys.Rev.B*, **63**, 201403R (2001).
- [8] M.Damnjanovic, I.Milosevic, T.Vukovic, and R.Sredanovic, *Phys.Rev.B*, **60**, 2728 (1999).
- [9] I.Milosevic, R.Zivanovic, and M.Damnjanovic, *Polymer*, **38**, 4445 (1997).
- [10] D.W.Brenner, *Phys.Rev.B*, **42**, 9458 (1990).
- [11] R.L.Flurry *Symmetry groups. Theory and chemical applications*, (Prentice-Hall, INC, New Jersey, 1980).
- [12] M.M.El'yashevich *Atomic and molecular spectroscopy*, (Editorial URCC, Moscow, 2001, in Russian).
- [13] E.B.Wilson, J.C.Decius, P.C.Cross *The symmetry of infrared and Raman vibrational spectra*, (McGraw-Hill Publishing Company LTD, New York, London, Toronto 1960).
- [14] R.Saito, T.Takeya, T.Kimura, G.Dresselhaus, and M.S.Dresselhaus, *Phys.Rev.B*, **59**, 2388 (1999).
- [15] E.Richter, K.R.Subbaswamy, *Phys.Rev.Lett.*, **79**, 2738 (1997).
- [16] M.Menon, K.R.Subbaswamy, and M.Sawtarie, *Phys.Rev.B*, **48**, 8398 (1993).
- [17] M.Menon, E.Richter, and K.R.Subbaswamy, *J.Chem.Phys.*, **104**, 5875 (1996).

TABLES

TABLE I. The vibrational spectrum of (10,10) CNT calculated using the Brenner potential. The mode frequency ω (in cm^{-1}) and its symmetry S are given in the first and second columns. The polarization tensor elements $\alpha_{\xi\xi'}$ are also shown. Raman-active vibrations are underlined.

ω	S	$\alpha_{\xi\xi'}$	ω	S	$\alpha_{\xi\xi'}$	ω	S	$\alpha_{\xi\xi'}$
<u>12</u>	E_{2g}	$(\alpha_{xx} - \alpha_{yy}, \alpha_{xy})$	523	E_{1g}		1415	E_{9u}	
34	E_{3u}		530	A_u		1464	E_{8g}	
65	E_{4g}		558	B_g		1515	E_{7u}	
81	E_{9g}		571	E_{9u}		1561	E_{6g}	
102	E_{5u}		596	E_{4g}		1600	E_{5u}	
144	E_{6g}		605	E_{8g}		1632	E_{4g}	
<u>150</u>	A_{1g}	$\alpha_{xx} + \alpha_{yy}, \alpha_{zz}$	648	E_{7u}		1656	E_{3u}	
160	E_{8u}		692	E_{6g}		1662	A_u	
189	E_{7u}		715	E_{5u}		1663	E_{1g}	$(\alpha_{xz}, \alpha_{yz})$
211	E_{1u}		746	E_{5u}		1665	E_{2u}	
231	E_{8g}		774	E_{4g}		1669	E_{3g}	
236	E_{7g}		804	E_{3u}		<u>1673</u>	E_{2g}	$(\alpha_{xx} - \alpha_{yy}, \alpha_{xy})$
265	E_{9u}		826	E_{2g}		1673	E_{4u}	
279	A_g		840	E_{1u}		1677	E_{5g}	
307	E_{6u}		845	A_{2g}		1682	E_{6u}	
<u>331</u>	E_{2g}	$(\alpha_{xx} - \alpha_{yy}, \alpha_{xy})$	849	E_{6g}		1683	E_{1u}	
370	E_{5g}		961	E_{7u}		1685	E_{7g}	
425	E_{4u}		1060	E_{8g}		<u>1686</u>	A_{1g}	$\alpha_{xx} + \alpha_{yy}, \alpha_{zz}$
464	E_{3u}		1138	E_{9u}		1688	E_{8u}	
470	E_{3g}		1172	B_g		1690	E_{9g}	
503	E_{2u}		1391	B_g		1691	A_{1u}	

TABLE II. Raman-active modes of (n, n) and $(n, 0)$ CNT for $n = 9 - 12$ calculated using the Brenner's potential.

CNT	Frequencies (cm^{-1}) and symmetries of Raman-active modes
(9,9)	15 (E_{2g}), 167 (A_{1g}), 366 (E_{2g}), 1665 (E_{2g}), 1667 (E_{2g}), 1684 (A_{1g})
(10,10)	12 (E_{2g}), 150 (A_{1g}), 331 (E_{2g}), 1673 (E_{2g}), 1686 (A_{1g})
(11,11)	10 (E_{2g}), 137 (A_{1g}), 302 (E_{2g}), 1665 (E_{2g}), 1677 (E_{2g}), 1688 (A_{1g})
(12,12)	9 (E_{2g}), 125 (A_{1g}), 278 (E_{2g}), 1680 (E_{2g}), 1689 (A_{1g})
(9,0)	47 (E_{2g}), 286 (A_{1g}), 362 (E_{2g}), 591 (E_{2g}), 741 (E_{2g}), 1144 (E_{2g}), 1672 (E_{2g}), 1677 (A_{1g})
(10,0)	38 (E_{2g}), 258 (A_{1g}), 542 (E_{2g}), 1676 (E_{2g}), 1680 (A_{1g})
(11,0)	31 (E_{2g}), 235 (A_{1g}), 348 (E_{2g}), 499 (E_{2g}), 695 (E_{2g}), 1147 (E_{2g}), 1679 (E_{2g}), 1683 (A_{1g})
(12,0)	26 (E_{2g}), 216 (A_{1g}), 462 (E_{2g}), 1681 (E_{2g}), 1685 (A_{1g})

TABLE III. Symmetry operations for D_{nh} and D_{nd} point groups and symmetry operation for (n, n) CNTs. Here E is the unit operation; C_n^m is the rotation about the z-axis by angle $2\pi m/n$; C_2', C_2'', C_2''' are rotations about C_2', C_2'', C_2''' axes (see Fig. 3) by an angle π ; σ_h is the reflection in the plane perpendicular to the main symmetry axis; σ_v is reflection in the plane including the main symmetry and one of C_2 axes; σ_d is reflection in the plane which includes the principal axis and bisects the angle between two two-fold axes; S_n^m is the rotation about the principal axis by angle $2\pi m/n$ and reflection in the plane σ_h : $S_n^m = C_n^m \otimes \sigma_h$; i - is the inversion operation.

	D_{nh}	D_{nh}	D_{nd}	D_{nd}	CNT	CNT
	even n	odd n	even n	odd n	(n, n) even n	(n, n) odd n
E	+	+	+	+	+	+
$C_n^m, m = 1, \dots, n-1$	+	+	+	+	+	+
$S_n^m, m = 1, \dots, n-1$	+	+	-	-	+	+
$S_{2n}^m, m = 1, 3 \dots 2n-1$	-	-	+	+	+	+
σ_v	+	+	-	-	+	+
σ_h	+	+	-	-	+	+
σ_d	+	-	+	+	+	+
C_2'	-	-	+	+	+	+
C_2''	+	+	-	-	+	-
C_2'''	+	-	-	-	+	+
i	+	-	-	+	+	+

FIGURE CAPTIONS

Fig. 1. An example of B_g mode ($\omega = 1172 \text{ cm}^{-1}$) with “double” symmetry is shown as a side view of an armchair CNT with even n . The mode is antisymmetric with respect to rotation about C'_2 and C''_2 axes and is symmetric with respect to rotation about C'''_2 axis. Axes are perpendicular to the principal axis z . C'_2 , C''_2 and C'''_2 axis pass through centers of opposite horizontal bonds, centers of opposite hexagons, and centers of opposite slanted bonds, respectively.

Fig. 2. Zero-frequency modes: (a) A_{2g} – rotation about the principal axis; (b) B_{2u} – translation along the principal axis; (c) E_{1u} – translations along x and y axes perpendicular to the principal axis z .

Fig. 3. Unit cells of (6,6) (left column) and (5,5) (right column) CNTs with their symmetry elements. Top panels show unit cell chosen as a chain of hexagons; middle panels present armchair unit cells. The side view of tube fragments is given in the bottom panels.

Fig. 4. Schematic representation of non-zero polarization matrix elements in (x, y) section of CNTs: $\alpha_{xx} = a_n \cos^2 \phi + a_\tau \sin^2 \phi$, $\alpha_{yy} = a_\tau \cos^2 \phi + a_n \sin^2 \phi$, $\alpha_{xy} = \alpha_{yx} = \frac{1}{2} (a_n - a_\tau) \sin 2\phi$, $\alpha_{xx} - \alpha_{yy} = (a_n - a_\tau) \cos 2\phi$. Note the sign alternation for α_{xy} and $\alpha_{xx} - \alpha_{yy}$ components.

Fig. 5. Schematic representations of $E_{1g} - E_{9g}$ modes. Note the sign alternations in lobes of vibrational modes, representing the relative displacements of atoms from equilibrium positions.

Fig. 6. Top view (in the (x, y) -section of (10,10) CNT) of Raman-active A_{1g} modes: (a) “breathing” mode ($\omega = 150 \text{ cm}^{-1}$); (b) high-frequency tangential mode ($\omega = 1686 \text{ cm}^{-1}$).

Fig. 7. All E_{2g} modes for (10,10) CNT in the (x, y) plane: (a) $\omega = 12 \text{ cm}^{-1}$; (b) $\omega = 331 \text{ cm}^{-1}$; (c) $\omega = 826 \text{ cm}^{-1}$; (d) $\omega = 1673 \text{ cm}^{-1}$.

Fig. 8. (a) Armchair unit cell of (6,6) CNT; (b) unit cell projection on the plain; (c) Schematic representation of the unit cell as a linear chain (with cyclic boundary conditions), where every pair of atoms of one layer is substituted by one unit (the vibrational mode for $k = 2$ is shown); (d) representation of this mode in polar coordinates.

Fig. 9. Components of electric field and polarization vectors in the cross-section of CNT for different polar angles ϕ .

FIGURES

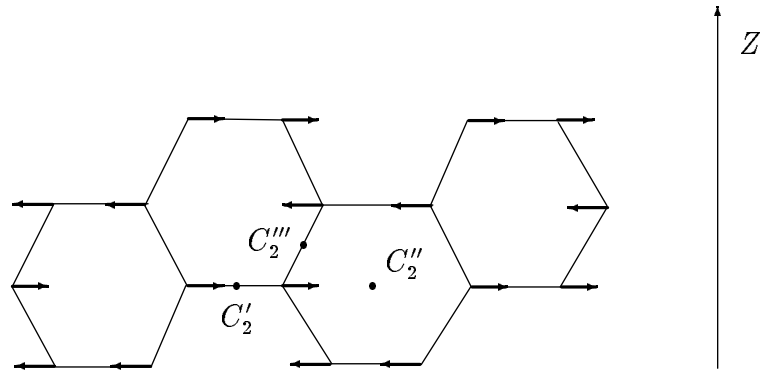
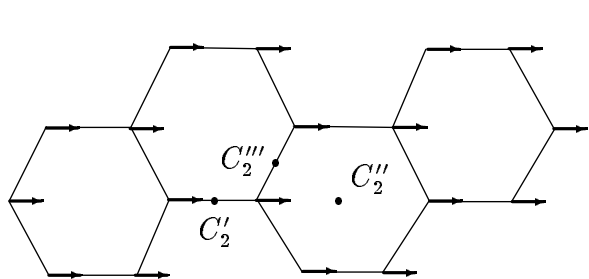
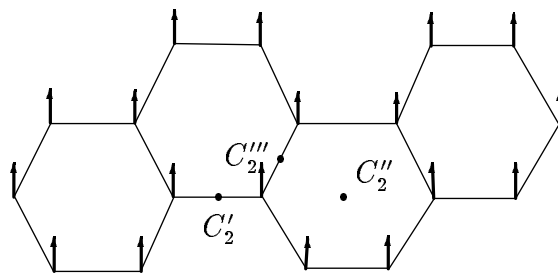


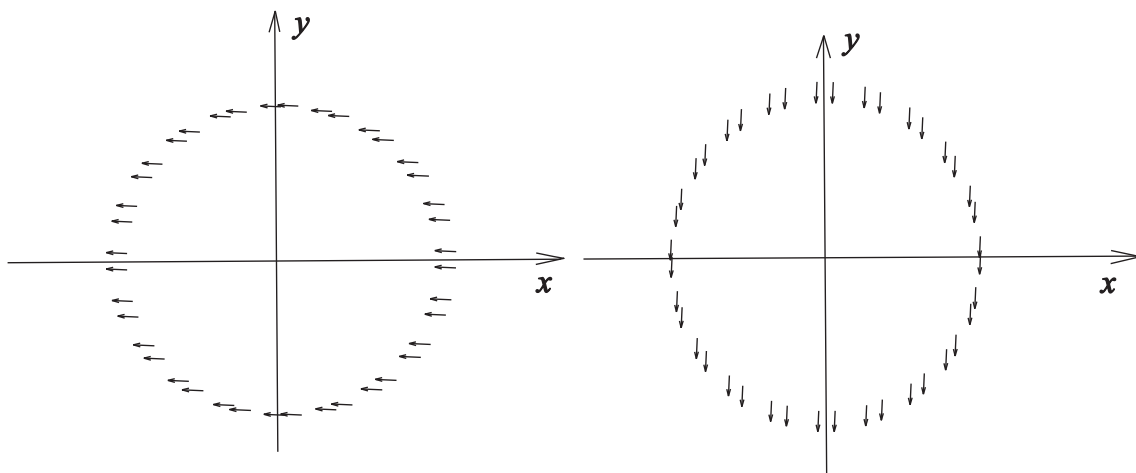
FIG. 1.



a



b



c

FIG. 2.

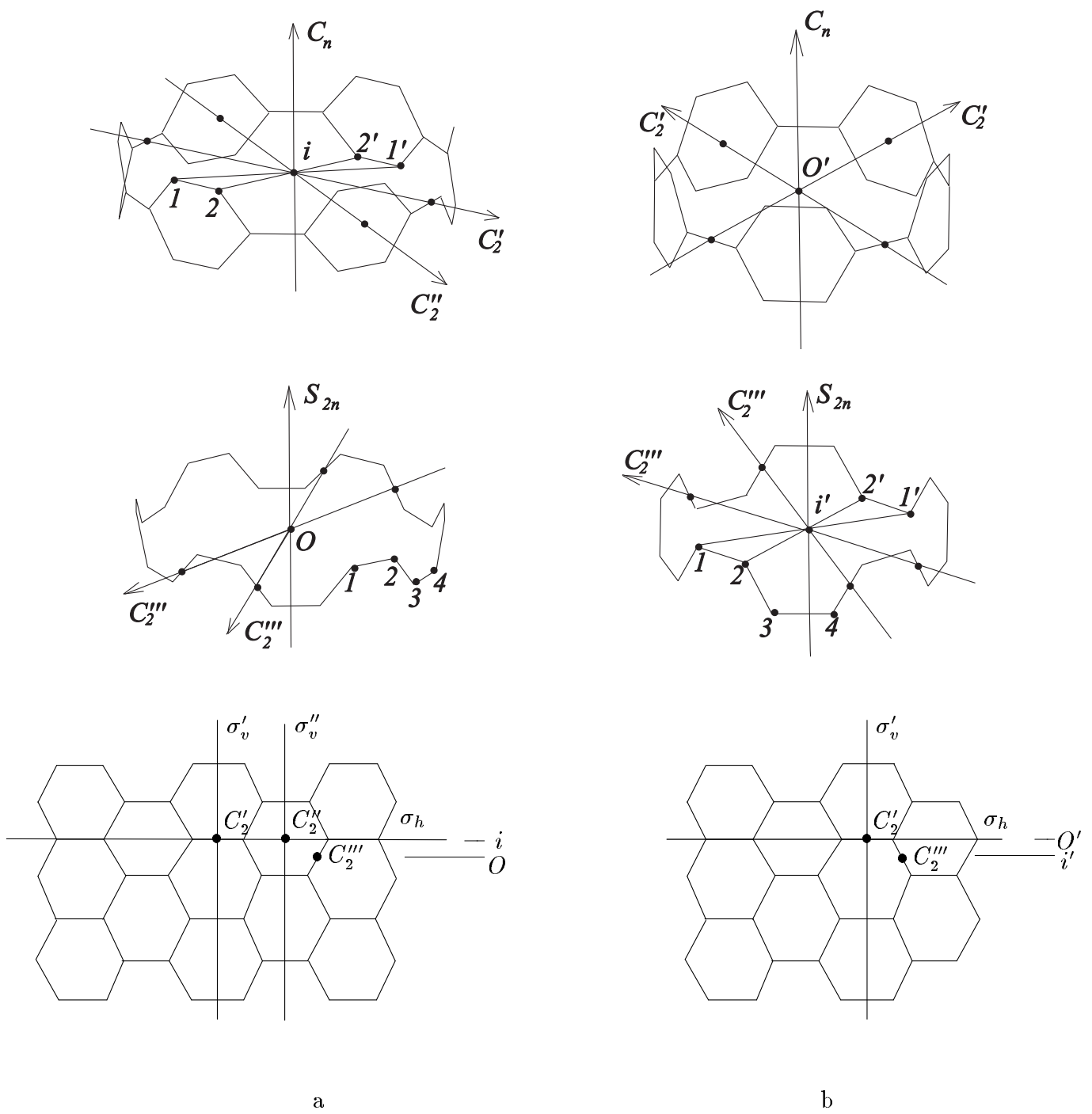


FIG. 3.

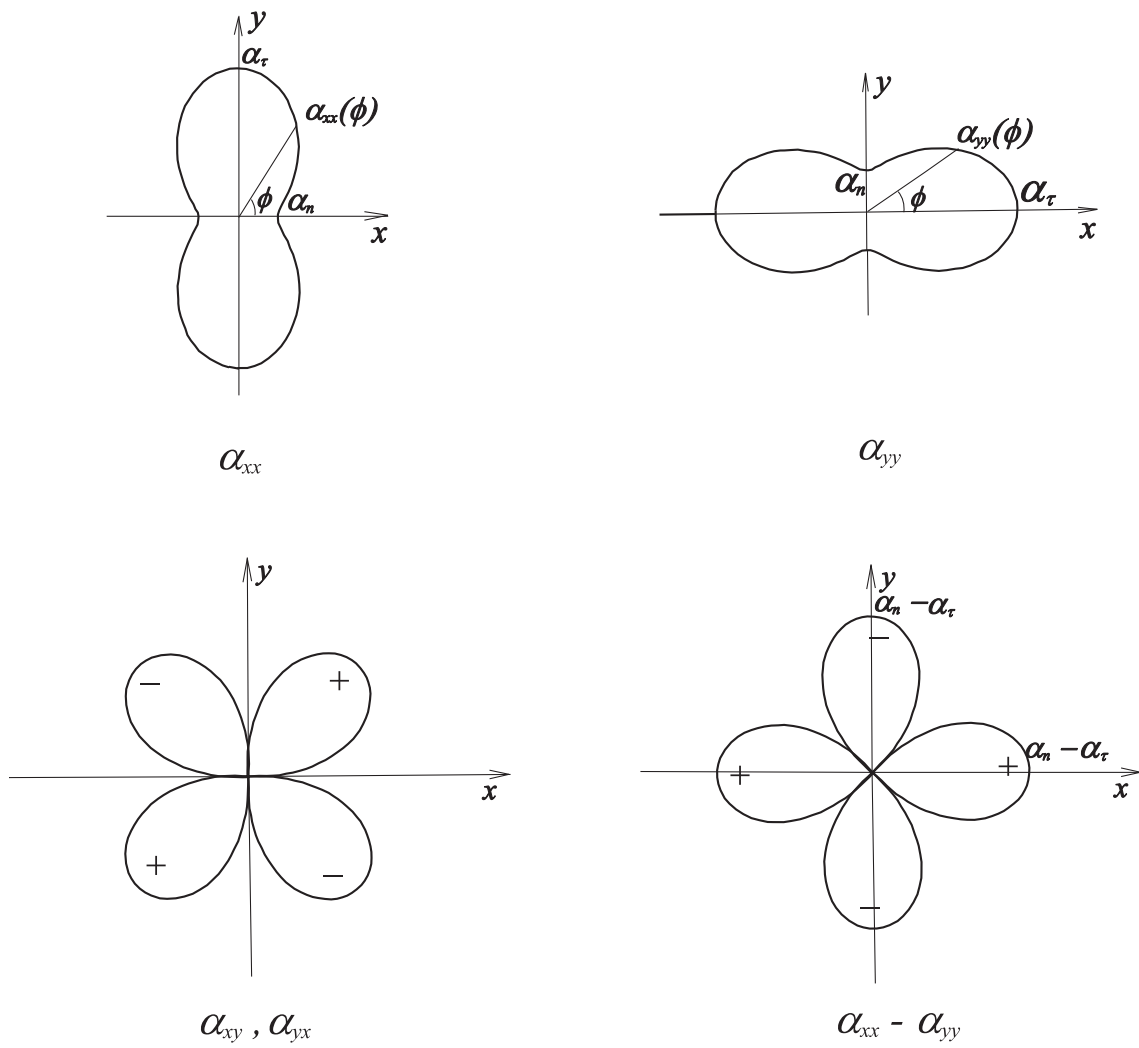


FIG. 4.

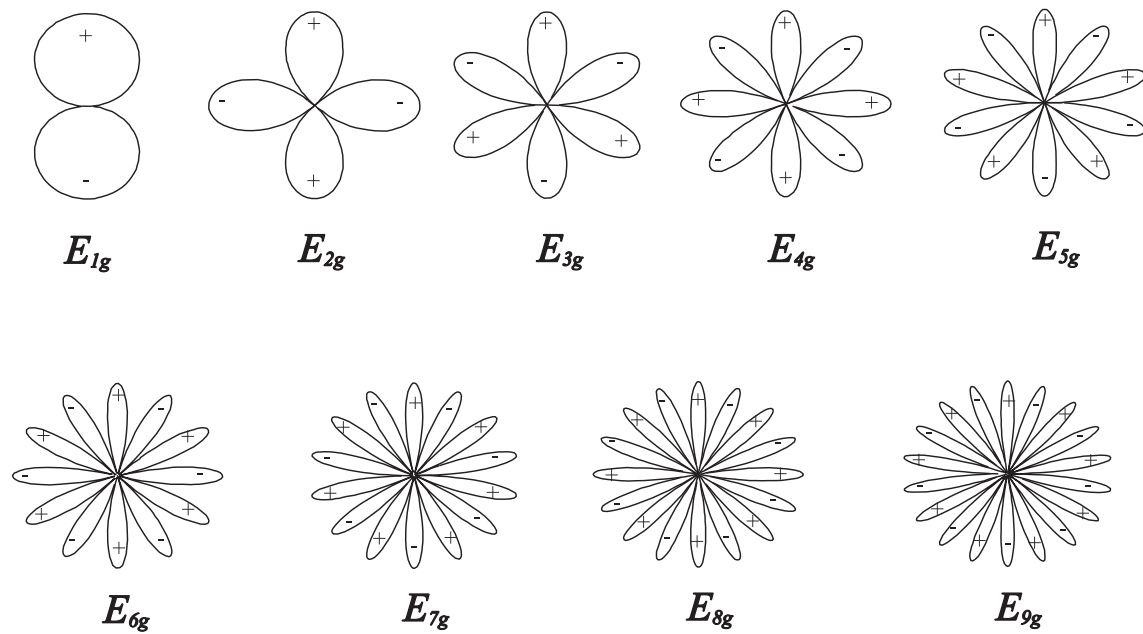
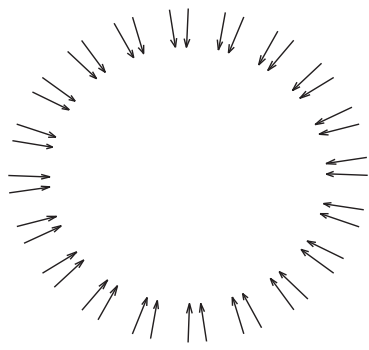
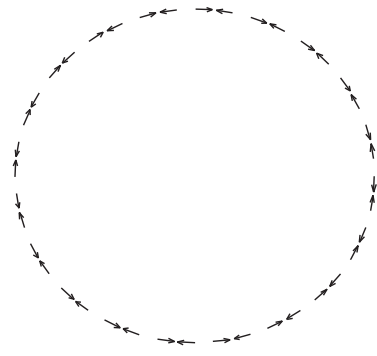


FIG. 5.

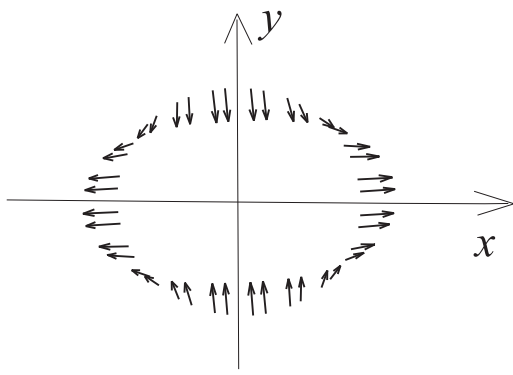


a

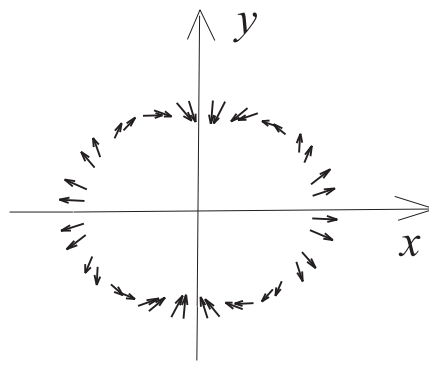


b

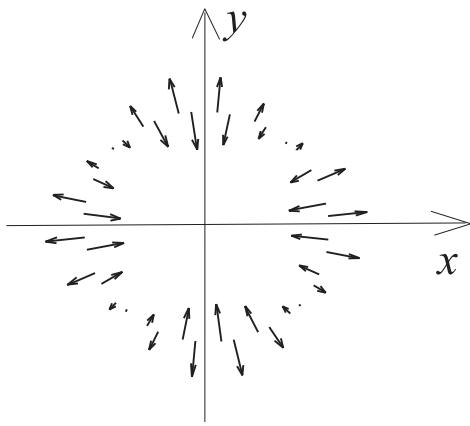
FIG. 6.



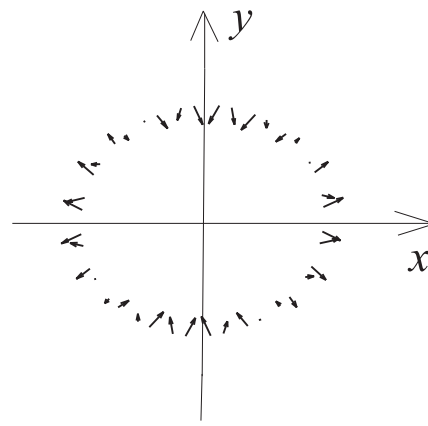
a



b



c



d

FIG. 7.

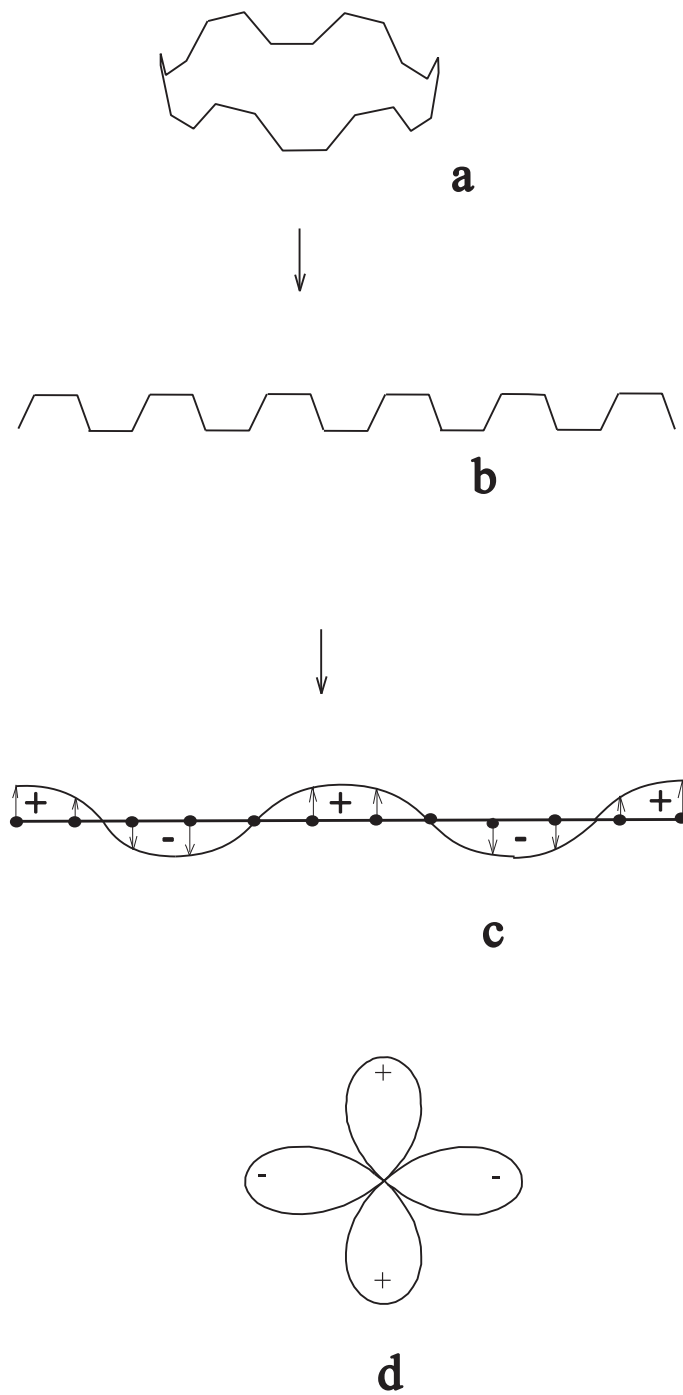


FIG. 8.

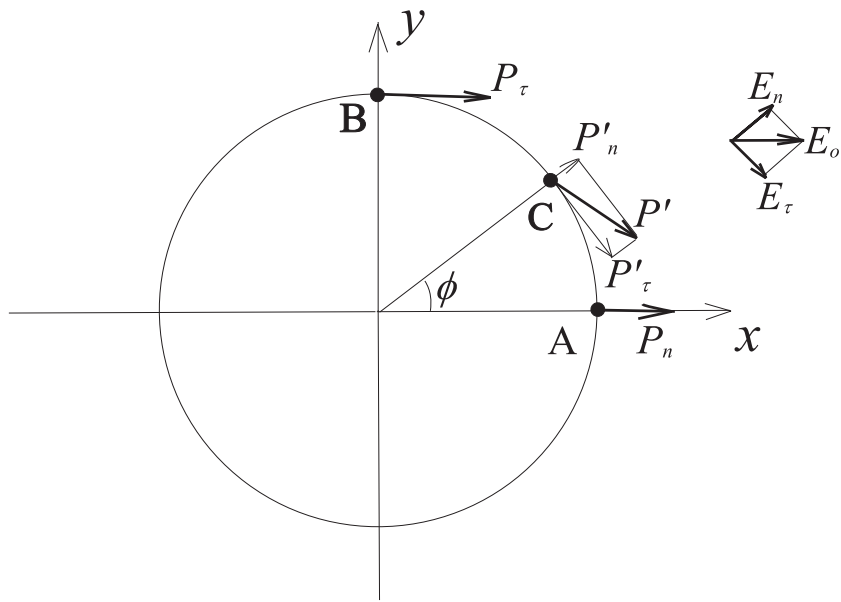


FIG. 9.